Influence of the Mass Transfer Model on the Numerical Prediction of the Cavitating Flow Around a Marine Propeller

Mitja Morgut[1], Enrico Nobile[1]

[1]Dipartimento di Ingegneria Meccanica e Navale, University of Trieste, Trieste, Italy

ABSTRACT

Cavitating flows, which can occur in a variety of practical applications, can be modelled using a wide range of methods. One strategy consists of using the RANS (Reynolds Averaged Navier Stokes) approach along with an additional transport equation for the liquid volume fraction, where mass transfer rate due to cavitation is modelled by a mass transfer model.

In this study, we verify the influence of three widespread mass transfer models, mainly on the numerical predictions of the propeller performances. The models in question share the common feature of employing some empirical coefficients to tune the models of condensation and evaporation processes, which can influence the accuracy and stability of the numerical predictions. For this reason, and for a fair and congruent comparison, the empirical coefficients of the different mass transfer models are first equally well tuned using an optimization strategy.

The numerical predictions of the propeller performances based on the three different well-tuned mass transfer models are very close to each other. Unfortunately, the numerical cavitation patterns are slightly overestimated compared to the experimental ones, and the thrust breakdown is not properly predicted either.

Finally, we roughly verify that for the prediction of the model scale propulsive performances in the presence of the partial and tip vortex cavitation, the turbulence model, among those considered in this study, plays a minor role.

Keywords

Propeller, cavitation, mass transfer model

1 INTRODUCTION

Owing to the continuous improvements of CFD (Computational Fluid Dynamics) technologies and steady increase of computer performances, numerical simulations are nowadays extensively used for design purposes, allowing the experimental tests to be performed only at the final stages of the project. With reference to marine applications, the CFD approach is today widely used for the hull and propeller design. However, a successful CFD procedure is determined by many factors, such as: CAD geometry, topology and dimension of the computational domain, meshing strategy, and physical modelling.

Referring to the physical modelling, in this study we investigated the influence of the mass transfer model on the numerical predictions of the cavitating flow around a marine propeller. The study was carried out using the ANSYS-CFX 12 (which will be referred to from now as, CFX) commercial CFD solver.

To this aim, we considered the Zwart et al (2004) model, and the models inspired by the works of Kunz et al (2000) and Singhal et al (2002) respectively. The Zwart model is the native model of CFX, while the other two were added to CFX. All these models share the common feature of employing some tuneable parameters to adjust the evaporation and condensation processes, which can markedly affect the accuracy of the predictions.

For this reason, the different models were first equally well tuned, by means of an optimization strategy, considering the two-dimensional sheet cavity flow around the NACA66MOD hydrofoil.

Successively, the well-tuned mass transfer models were used to evaluate the influence of the mass transfer model on the numerical predictions of the cavitating flow around a marine propeller in uniform inflow. The computational results obtained with the calibrated mass transfer models were very close to each other, thus demonstrating the reliability and robustness of the calibration process. However, the extents of the numerical cavitation patterns were slightly overestimated compared to the numerical ones, and the thrust breakdown was not properly predicted.

Moreover, we also roughly verified the influence of the turbulence modelling on the numerical predictions of the propeller performances. For this aim, and for a particular regime, we also used, in addition to the two equation Shear Stress Transport (SST) turbulence model (Menter 1998), the computationally more expensive, second order Baseline Reynolds Stress Model (BSL-RSM) (ANSYS 2010). No significant differences were observed between the results obtained with the two turbulence models.

In the following, we first describe the mathematical model employed in the present study, followed by the description of the optimization strategy we developed for the calibration of the different mass transfer models. Then the comparison of the well-tuned mass transfer models for the

numerical prediction of the flow around a marine propeller is provided. At the end, our concluding remarks are given.

2 MATHEMATICAL MODEL

Cavitating flows can be modelled using different methods. In the present study, we used a homogeneous multiphase transport equation based model (Bouziad 2006) which will be described in the following section. Moreover, for an exhaustive review of other methods, available in the literature and not provided here, we refer, for instance, to the work of Koop (2008).

2.1 Governing Equations

In the homogeneous multiphase transport equation based model, the cavitating flow can be described by the following set of governing equations:

$$\begin{cases} \nabla \cdot \boldsymbol{U} = \dot{m}\left(\frac{1}{\rho_l} - \frac{1}{\rho_v}\right) \\ \frac{\partial(\rho \boldsymbol{U})}{\partial t} + \nabla \cdot (\rho \boldsymbol{UU}) = -\nabla P - \nabla \cdot \boldsymbol{\tau} + S_M \\ \frac{\partial \gamma}{\partial t} + \nabla \cdot (\gamma \boldsymbol{U}) = \frac{\dot{m}}{\rho_l} \end{cases} \qquad (1)$$

Cavitating flow is modelled as a mixture of two species i.e. vapour and liquid behaving as one. The phases are considered incompressible and share the same instantaneous velocity $\boldsymbol{U}$ and pressure fields P. The derivation of governing equation can be found in Zwart et al (2004).

The above equations are, in order, the continuity and the momentum equation for the liquid-vapour mixture, and the volume fraction equation for the liquid phase. $\boldsymbol{\tau}$ is the stress tensor, S_M stays for the additional sources of momentum, (for instance the Coriolis and centrifugal forces in the rotating frame of reference), $\dot{m}$ (kg/m^{3}s) is the interphase mass transfer rate due to cavitation, ρ_v (kg/m^3) the vapour density, ρ_l (kg/m^3) the liquid density.

The water volume fraction γ and the vapour volume fraction α are defined as follows:

$$\gamma = \frac{volume\ liquid}{total\ volume} \qquad \alpha = \frac{volume\ vapour}{total\ volume} \qquad (2)$$

and are related to each other through the following relevant constitutive relationship:

$$\gamma + \alpha = 1 \qquad (3)$$

Finally, ρ (kg/m^3) and μ (kg/m s) are the density and the dynamic viscosity of the vapour-water mixture, scaled by the water volume fraction, respectively.

$$\begin{cases} \rho = \gamma \rho_l + (1-\gamma)\rho_v \\ \mu = \gamma \mu_l + (1-\gamma)\mu_v \end{cases} \qquad (4)$$

The specific interphase mass transfer rate $\dot{m}$ can be modelled using an appropriate mass transfer model, also called cavitation model.

If the turbulent flow is modelled using the RANS approach, in the above equations $\boldsymbol{U}$ and P stands for the statistically averaged velocity and pressure fields, respectively. Moreover, in the momentum equation additional Reynolds Stress terms appear (Versteeg & Malalasekera 2007). These terms can be modelled using an eddy viscosity approach such as the k-ε or SST turbulence model, or using a second moment closure model such as the BSL-RSM turbulence model (which will be referred from now on as RSM).

In the following, we provide a brief description of the three different mass transfer models compared in this study, where the interphase mass transfer rate due to cavitation was assumed positive if directed from vapour to water.

2.2 Mass Transfer Models

2.2.1 Zwart Model

The Zwart model is the native CFX mass transfer model. It is based on the simplified Rayleigh-Plesset equation for bubble dynamics (Brennen 1995):

$$\dot{m} = \begin{cases} -F_e \dfrac{3r_{nuc}(1-\alpha)\rho_v}{R_B}\sqrt{\dfrac{2}{3}\dfrac{P_v - P}{\rho_l}} & if\ P < P_v \\ F_c \dfrac{3\alpha\rho_v}{R_B}\sqrt{\dfrac{2}{3}\dfrac{P - P_v}{\rho_l}} & if\ P > P_v \end{cases} \qquad (5)$$

In the above equations, P_v is the liquid vapour pressure, r_{nuc} the nucleation site volume fraction, R_B the radius of a nucleation site, F_e and F_c are two empirical calibration coefficients for the evaporation and condensation processes, respectively. In CFX the above mentioned coefficients, by default, are set as follow: $r_{nuc}=5\text{x}10^{-4}$, $R_B=1.0\text{x}10^{-6}$m, $F_e=50$, $F_c=0.01$. Moreover, from the above equations it can be seen that expressions for condensation and evaporation are not symmetric. In particular, it is possible to recognise that in the expression for evaporation α is replaced by $r_{nuc}(1-\alpha)$ to take into account that, as the vapour volume fraction increases, the nucleation site density must decrease accordingly.

2.2.2 Full Cavitation Model

The mass transfer model proposed by Singhal et al (2002) originally known as Full Cavitation Model (for the sake of brevity FCM), is currently employed in some commercial CFD codes, for instance FLUENT (www.ansys.com) and PUMPLINX (www.simerics.com). This model is also based on the reduced form of the Rayleigh-Plesset equation for bubble-dynamics, and its formulation states as follows, where f_v is the vapour mass fraction, k (m^2/s^2) the turbulent kinetic energy, T (N/m) the surface tension, $C_e=0.02$ and $C_c=0.01$ are two empirical calibration coefficients.

$$\dot{m} = \begin{cases} -C_e \dfrac{\sqrt{k}}{T}\rho_l\rho_v\sqrt{\dfrac{2}{3}\dfrac{P_v - P}{\rho_l}}\left(1-f_v\right) & if\ P < P_v \\ C_c \dfrac{\sqrt{k}}{T}\rho_l\rho_l\sqrt{\dfrac{2}{3}\dfrac{P - P_v}{\rho_l}}f_v & if\ P > P_v \end{cases} \qquad (6)$$

It is important to note that in this work, for convenience, we did not use the original formulation of the model, but the formulation derived by Huuva (2008) in which the vapour mass fraction f_v was replaced by the vapour volume fraction α.

2.2.3 Kunz Model

The Kunz mass transfer model is based on the work of Merkle et al (1998) and is currently one of the mass transfer models implemented in the OpenFOAM CFD Open Source Library (www.OpenFOAM.com). In this model, unlike the above mentioned models, the mass transfer is based on two different strategies for creation $\dot{m}^+$ and destruction $\dot{m}^-$ of liquid. The transformation of liquid to vapour is evaluated as being proportional to the amount by which the pressure is below the vapour pressure. The transformation of vapour to liquid, otherwise, is based on a third order polynomial function of volume fraction γ. The specific mass transfer rate is defined as $\dot{m} = \dot{m}^+ + \dot{m}^-$.

$$\begin{cases} \dot{m}^+ = \dfrac{C_{prod}\rho_v \gamma^2 (1-\gamma)}{t_\infty} \\[2mm] \dot{m}^- = \dfrac{C_{dest}\rho_v \gamma \min[0, P - P_v]}{(0.5\rho_l U_\infty^2)t_\infty} \end{cases} \quad (7)$$

In the above equations, U_∞ (m/s) is the reference velocity, $t_\infty = L/U_\infty$ is the mean flow time scale, where L is the characteristic length scale. C_{prod} and C_{dest} are two empirical coefficients. In the original formulation $C_{prod}=100$, $C_{dest}=100$.

3 TUNING OF MASS TRANSFER MODELS

As previously described, all the different mass transfer models examined in this study employ some empirical coefficients which can markedly influence the mass transfer process due to evaporation and condensation. This means that the accuracy of the specific mass transfer model is strictly related to the proper calibration of its empirical values.

3.1 The idea of the optimization strategy

In order to compare the models in the most congruent and fairest manner, we tried to bring all the models to the same level of accuracy through the tuning of their empirical coefficients.

To this aim, we developed an optimization strategy based on the modeFRONTIER 4.2 optimization framework (www.esteco.com). It is important to point out that with the developed strategy we did not tune the empirical coefficients considering the propeller case, but investigating the two-dimensional sheet cavity flow around the NACA66MOD hydrofoil (Shen & Dimotakis 1989). In this way, due to the minor computational costs we could explore, in a reasonable time and with limited computational resources, a significant number of coefficients' combinations. Moreover, in such a way we also had the opportunity to verify if the coefficients, calibrated for the hydrofoil case, could have a general

character thus ensuring the same order of accuracy also for the propeller case.

In order to properly tune the mass transfer models, we searched the couple of empirical coefficients which minimized the objective function f.

$$f = \sum_\sigma \sum_{i=1}^N \left| C_{Pi} - C_{Pi,\exp} \right| \qquad \sigma = 1.00, 0.91, 0.84 \quad (8)$$

The objective function f was defined as the sum of the differences between the numerical C_{Pi} and experimental $C_{Pi,exp}$ values of the pressure coefficient, and σ the cavitation number to be defined later. The pressure was measured (computed) at the $N=12$ locations along the suction side of the NACA66(MOD) hydrofoil, for three different cavitating flow regimes at an angle of attack AoA=4°.

In order to find a couple of values which minimized the function f for each model, we initially explored the design space using the MOGA-II, multi objective genetic optimization algorithm (ESTECO 2009). The search started from a DOE (Design of Experiments) of ten designs randomly generated. The MOGA-II was then run for ten generations. Next, in order to refine the solution, the Simplex (Rao 1996) single objective optimization algorithm was used, starting from the three best solutions obtained with MOGA-II. However, in this case, no significant differences were observed between the best solutions obtained with Simplex and MOGA-II algorithms, respectively. For clarity, the logic of the optimization strategy is depicted in Fig. 1, where the optimizer block stays for both the MOGA-II and Simplex algorithms, and where ($X1$, $X2$) represents the couple of empirical coefficients for all three mass transfer models.
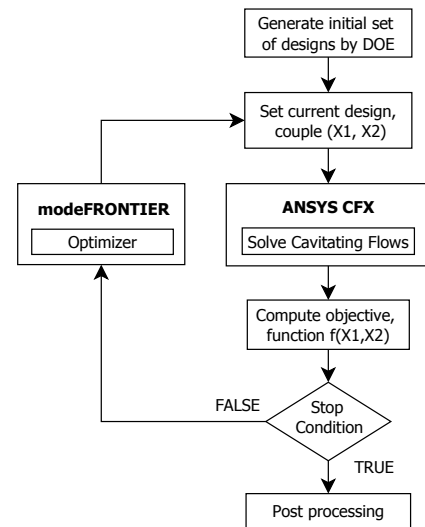

Figure 1: Logic of the optimization strategy for tuning the empirical coefficients of the mass transfer models

3.2 Numerical Strategy

In order to simulate the flow around the hydrofoil, we used a rectangular domain with Inlet and Outlet boundaries placed 3 chord lengths ahead of the leading

edge, and 5 chord lengths behind the trailing edge of the hydrofoil, respectively. Moreover, in order to match the vertical extent of the experimental test section, the tunnel walls were placed 2.5 chord lengths from the hydrofoil. The hydrofoil considered in this study had a chord c=0.15m.

In order to simulate the flow, the following boundary conditions were applied: on solid surfaces (Tunnel walls, Hydrofoil surface) the no-slip condition was applied. On the Outlet boundary a fixed static pressure was imposed and on the side faces the symmetry condition was enforced. On the Inlet boundary, the values of the free-stream velocity components and turbulence quantities were fixed. Water and vapour volume fractions were set equal to 1 and 0, respectively. In order to match the experimental setup, during the computational studies the same Reynolds number was used. Since the water kinematic viscosity was ν_l= 8.92x10^{-7} (m^2/s), the free stream velocity was set to U = 12.2 (m/s). Assuming a turbulence intensity of 1%, the turbulent kinetic energy k and the turbulent dissipation rate were set equal to k = 0.0223 (m^2/s^2), ε = 0.1837 (m^2/s^3) respectively. In all simulations the water and vapour density were kept constant and equal to ρ_l = 997 (kg/m^3), ρ_v = 0.02308 (kg/m^3). Different cavitating flow regimes related to the cavitation (or Thoma) number σ, were defined varying the value of the saturation pressure P_v. This is because P_{ref}, U_∞ were kept constant and σ was defined as:

$$\sigma = \frac{P_{ref} - P_v}{0.5 \rho_l U_\infty^2} \qquad (9)$$

The Simulations were carried out using the commercial CFD solver ANSYS-CFX 12. It employs the node-centred finite volume method (more precisely the Control Volume-Based Finite Element Method - CVFEM) (Schneider & Raw, 1987). It uses a coupled solver, accelerated by an Algebric Multigrid, to solve the hydrodynamic equations (for u, v, w, p) as a single system, with a fully implicit discretization of the equations at any given time-step.
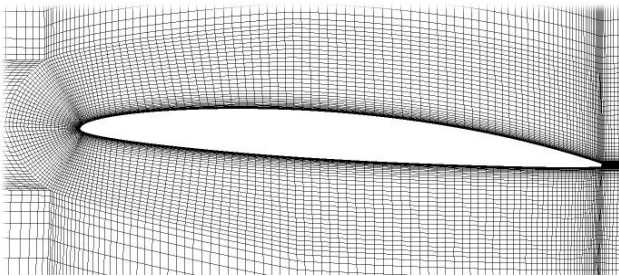

Figure 2: Mesh around the NACA66MOD hydrofoil

All the simulations were performed on an hexahedral grid with 58700 nodes, which proved to give mesh independent results (Morgut et al 2010) with an average value of y$^+$≅28 on the solid surfaces of the hydrofoil, where $y^+ = \mu_\tau y / \nu$ with $\mu_\tau = (\tau_w / \rho_l)^{1/2}$ the friction velocity, y the normal distance from the wall, τ_w the wall shear stress. The mesh was generated using the meshing

tool ANSYS ICEM CFD. In Fig. 2 the mesh around the hydrofoil is visible. For turbulence closure, the standard k-ε turbulence model in combination with scalable wall functions was employed.

3.3 Results and Discussion

In the case of the Zwart model, only the evaporation F_e and the condensation F_c coefficients were tuned within the ranges: $30 \leq F_e \leq 500$, $5.0x10^{-4} \leq F_c \leq 8.0x10^{-2}$. The other physical parameters of the model: r_{nuc}, R_B were kept constant and equal to the default values. The best result was found with F_c = 0.03 and F_e = 300.

For FCM, the values of the evaporation coefficient C_e and of the condensation coefficient C_c were tuned within the ranges: $0.01 \leq C_e \leq 1$, $1.0x10^{-6} \leq C_c \leq 1.0x10^{-2}$. The best solution was found with C_e = 0.40 and C_c = 2.30x10^{-4}.

Finally, for the Kunz model, C_{dest} and C_{prod} were tuned within the ranges: $100 \leq C_{dest} \leq 5000$, $10 \leq C_{prod} \leq 1000$ with t_∞=c/U_∞≅0.01s. The best solution was achieved with C_{prod} = 455 and C_{dest} = 4100.

In Table 1, for clearness, the tuned empirical values for all the three different models are collected, while in Fig. 3, the pressure distributions along the suction side of the NACA66(MOD) hydrofoil, computed with the tuned mass transfer models, for three value of cavitation onset, are compared with the experimental measurements. From the figure it is possible to note that the results obtained with different well-tuned mass transfer models were very close to each other and in line with the experimental data.

Table 1: Tuned empirical coefficients of the three different mass transfer models considered in the present study

Zwart		FCM		Kunz	
F_e	F_c	C_e	C_c	C_{dest}	C_{prod}
300	0.03	0.40	2.3x10^{-4}	4100	455

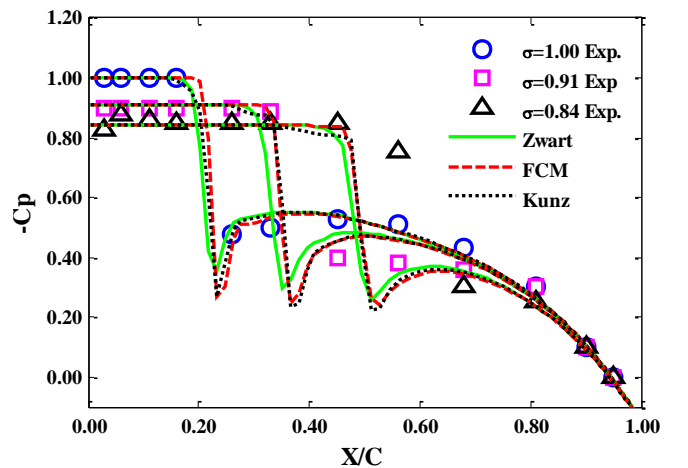**Figure 3: Pressure distributions along the suction side of the NACA66MOD hydrofoil at AoA=4° and Re=2x10^6.**

In the following, we present the predictions of the cavitating flow around the model scale propeller E779A

obtained using the different, equally well-tuned mass transfer models illustrated earlier.

4 PROPELLER E779A

The study of the influence of the mass transfer models on the numerical predictions of the flow around a marine propeller was carried out investigating the cavitating flow around the model scale propeller E779A. This propeller, belonging to INSEAN, is extensively used for the validation of CFD codes (Pereira et al 2004, Vaz 2005, Salvatore et al 2009, Gaggero 2010). E779A is a four-bladed, fixed-pitch, low-skew propeller designed in 1959 with a diameter of D=0.227m. Since 1997, it has been used in experimental activities performed by INSEAN aimed at providing a thorough characterization of marine propeller hydrodynamics and hydroacoustics over a wide range of operational conditions.
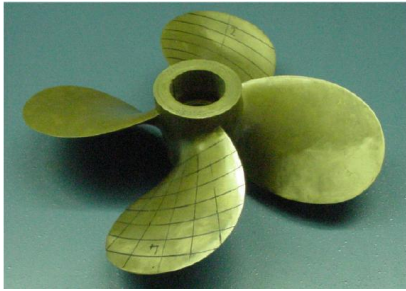
Figure 4: Model scale propeller E779A

4.1 Numerical Strategy

In this study, we simulated the flow around the propeller working in the homogenous uniform inflow. For this reason, due to the periodicity of the problem, numerical simulations were carried out considering only one passage blade and employing the MRF (Multiple Reference Frame) approach. The domain was defined, as illustrated in Fig. 5, by a segment of a cylinder, covering only one blade, and was moreover subdivided into a rotating part *Rotating* and into a stationary part *Fixed*. The dimensions of the domain are given in Table 2, where the variable Lmid, not visible in Fig. 5, is the axial length of the *Rotating* part, and D is the propeller diameter. The Inlet, Outlet and Outer boundaries of the *Fixed* part were placed far enough from the propeller in order to not markedly affect the results. The distances were set through a domain independence study, carried out considering more shapes of the *Fixed* part, and defined varying systematically L1, L2, and R2.

In order to simulate the flow, the following boundary conditions were set: On the Inlet boundary the turbulence intensity of 1% and free stream velocity components were set. On the outlet boundary fixed value of static pressure was imposed. On the periodic boundaries (sides of the domain) the rotational periodicity was ensured. On all solid surfaces the no slip boundary condition was applied, and on the radial Outer boundary the slip condition was imposed. In this case, for turbulence closure, the two equation SST turbulence model and also the second order

Table 2: Domain dimensions

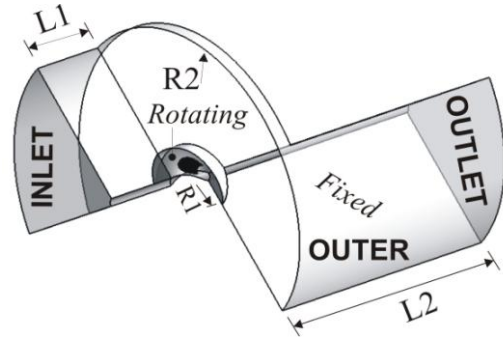|	R1	Lmid	R2	L1	L2
Rotating	0.70D	0.76D			
Fixed			5D	3D	5D

Figure 5: Geometry of the domain

BSL-RSM turbulence model were used, both available in ANSYS-CFX, in combination with the automatic wall treatment.

For a given value of the advance coefficient $J=U/nD$, the different cavitating flow regimes, determined by the cavitation number, σ_n, were defined varying the value of the saturation pressure P_v. This is because P_{ref}, ρ_l were kept constant and σ_n was defined, in this case, as:

$$\sigma_n = \frac{P_{ref} - P_v}{0.5\rho_l(nD)^2} \qquad (10)$$

where $P_{ref} = P_{outlet}$, and n (rps) was the rotational speed of the propeller.

4.2 Meshing

Also in this case, the meshes were generated with ANSYS-ICEM CFD. The part *Rotating* was discretized by a hexahedral mesh. It was generated, as done by other authors, for example (Abdel-Maksoud et al 1998; Berchiche & Janson 2008), decomposing the *Rotating* part in a large number of blocks. The resolution and also the quality of the cells were set through a proper node distribution on the edges of the blocks. For part *Fixed*, on the other hand, we used a hybrid-unstructured approach. This is because, due to the particular shape of domain, using the hexa-structured approach, the decomposition of the domain in blocks led to highly distorted elements in the twisted region - over the *Rotating* close to the Outer boundary. Moreover, since the detailed study of the flow field was far beyond the scope of the present work, the use of the more diffusive hybrid-unstructured mesh (Morgut & Nobile 2009), for *Fixed*, was expected not to significantly affect the accuracy of the results. The meshes used in this study proved to ensure mesh independent results for the prediction of the propeller performances. In particular, the mesh for *Rotating* had 645k nodes and for *Fixed* had 163k nodes. The average value of y^+ on the blade and hub surfaces was approximately 38. The two distinct parts of the domain were joined together in ANSYS CFX through the use of the GGI interfaces and

the frozen rotor frame change/mixing model (ANSYS 2010). In Fig. 6 the suction side blade surface mesh is visible.
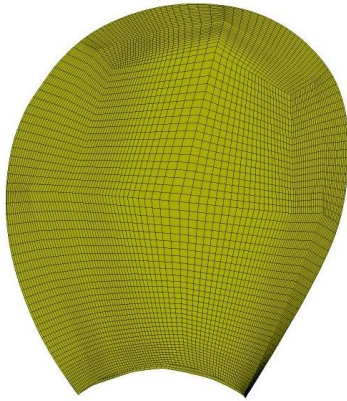

**Figure 6: Blade surface mesh**

4.3 Results and Discussion

Before illustrating the results, we point out that in this case for the Kunz mass transfer model we varied the value of t_∞ accordingly to the operational conditions. In particular, we set the value of t_∞ as

$t_\infty = C_{0.7R} / (\sqrt{U^2 + (2\pi n 0.7R)^2})$ where, $C_{0.7R}$ was the propeller blade chord at 70% of the propeller radius R and U the incoming freestream velocity. The numerical simulations were carried out following the experimental setup (Salvatore, personal communication and Salvatore et al. 2009). All the simulations were carried out using the SST turbulence model, but for a particular operating condition (i.e., (J=0.71, σ_n= 1.763) the RSM model was also tested).

To follow in Fig. 7, we qualitatively compared the cavitation patterns, depicted as isosurfaces of vapour volume fraction α=0.5, predicted using alternatively all the three different mass transfer models in combination with the SST turbulence model, for three different operational conditions, i.e. (J=0.71, σ_n= 1.763); (J=0.77, σ_n=1.783); (J=0.83, σ_n=2.063).
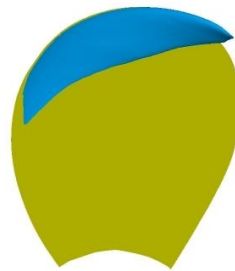
From Fig. 7, it is possible to see that in this case the results obtained with the three different mass transfer models were also very close to each other but the numerical cavitation patterns were slightly overestimated compared to the experimental ones.
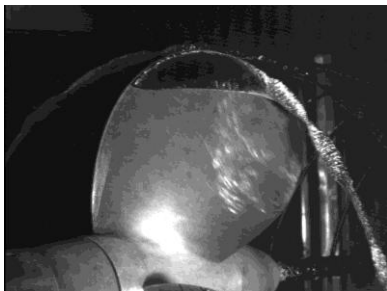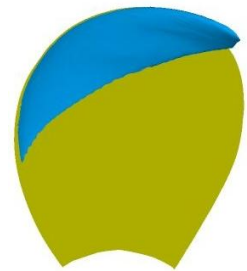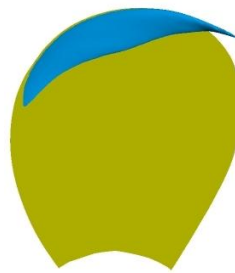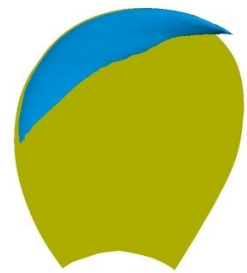

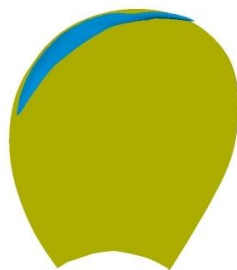| Exp, J=0.71 σ_n=1.763 | Zwart | FCM | Kunz |

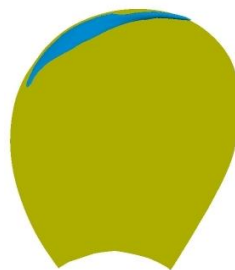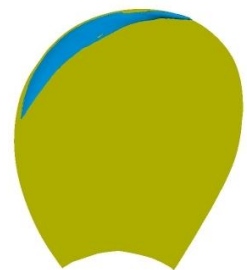| Exp, J=0.77 σ_n=1.783 | Zwart | FCM | Kunz |

| Exp, J=0.83 σ_n=2.063 | Zwart | FCM | Kunz |
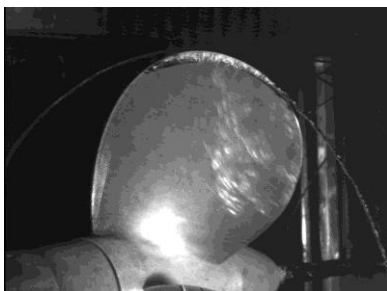
Figure 7: Cavitation patterns, depicted as isosurfaces of the vapour volume fraction α=0.5 obtained using different well-tuned mass transfer models in combination with the SST turbulence model.

For a quantitative comparison of results, we considered the global values of the problem represented by the thrust Kt, and torque Kq coefficients defined as:

$$Kt = \frac{T}{\rho_l n^2 D^4} \qquad Kq = \frac{Q}{\rho_l n^2 D^5} \qquad (11)$$

where T (N) was the thrust, Q (Nm) the torque. In Table 3, the numerical values for the cavitating regime J=0.71, σ_n=1.763 as well as for the non-cavitating regime are compared.

Table 3: Numerical results at J=0.71 for σ_n=1.763 and for the non-cavitating regime

Uniform Inflow	Non-Cavitating		Cavitating	
J=0.71	*Kt*	*10Kq*	*Kt*	*10Kq*
Measured(Tunnel)	0.256	0.464	0.255	0.460
Measured (O.W.)	0.238	0.429		
SST	0.246	0.442		
Zwart + SST			0.252	0.453
FCM + SST			0.249	0.446
Kunz + SST			0.253	0.453
RSM	0.247	0.441		
Zwart + RSM			0.252	0.450
FCM + RSM			0.249	0.443
Kunz + RSM			0.253	0.451

Table 3 shows us, that for this particular condition, the results associated with different mass transfer models were very close to each other and in line with results presented by other authors (Salvatore et al 2009), as well as with the experimental measurements. It is interesting to note that even though the cavity patterns were overestimated, the predicted values were very close to experimental ones. Similar trends were observed also for other two conditions (J=0.77, σ_n=1.783); (J=0.83 σ_n=2.063).

Finally, it is possible to notice that the differences between the computed values using the different turbulence models were minimal in both cavitating and non-cavitating regimes. Thus, from this rough comparison, it seems that for the overall prediction of the propeller performances in the presence of partial and tip vortex cavitation, the workhorse two-equation SST turbulence model can guarantee the same level of accuracy as the computationally more expensive BSL-RSM turbulence model.

In Fig. 8 and 9 the numerical results obtained for a wide range of operational conditions using alternatively the different mass transfer models in combination with the SST turbulence model are compared to each other and to the experimental data. From Fig. 8 and 9, it is possible to see that the results obtained using the different mass transfer models were very close to each

other. Unfortunately, the numerical simulations fail to predict accurately the performances providing, as observed by (Pereira et al 2004), a premature breakdown of the performances.
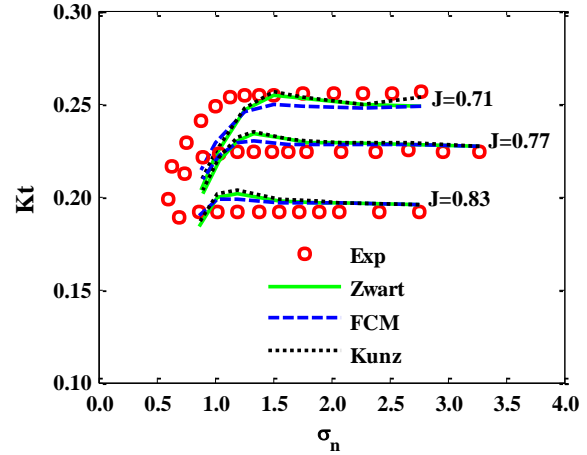
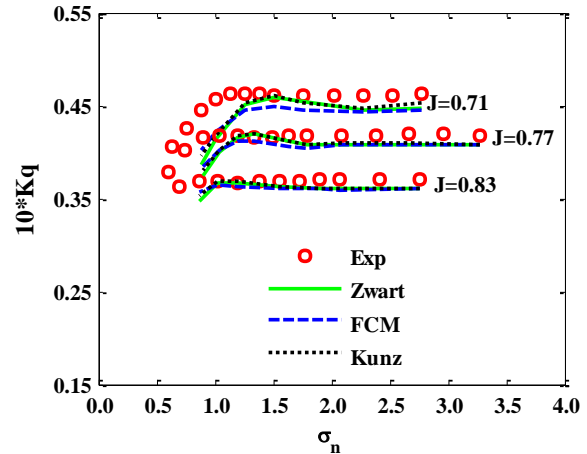**Figure 8: Influence of the cavitation number σ_n and of the mass transfer model on the thrust coefficient.**

Figure 9: Influence of the cavitation number σ_n and of the mass transfer model on the torque coefficient.

5 CONCLUDING REMARKS

With reference to marine applications, the CFD approach is today widely used for the hull and propeller design. However, a successful CFD procedure is determined by many factors, such as: CAD geometry, topology and dimension of the computational domain, meshing strategy, and physical modelling.

In this study, we investigated the influence of the mass transfer model on the numerical prediction of the model scale propeller performances. To this aim, we compared three widespread mass transfer models available in the literature. For a fair and congruent comparison, the three different models were equally well tuned by means of an optimization strategy, driven by the modeFRONTIER v.4.2 optimization framework. Simulations were carried out using the ANSYS CFX 12 commercial CFD solver and the meshes were generated with ANSYS ICEM CFD 12.

The computational results obtained, using alternatively the different well-tuned mass transfer models, were very close to each other. But numerical cavitation patterns were slightly overestimated compared to the experimental ones, and the thrust breakdown was not properly predicted.

Finally, for a particular operational condition we roughly verified that for the prediction of the propeller performances in the presence of partial and tip vortex cavitation, the turbulence model plays a minor role.

REFERENCES

Abdel-Maksoud, M., Menter, F. R. & Wuttke, H. (1998). 'Viscous Flow Simulations for Conventional and High-Skew Marine Propellers'. Schiffstechnik/Ship Technology Research **45**(2), p.p. 64-71.

ANSYS (2010) 'CFX-Solver Theory Guide', Rel. 12.

Berchiche, N. & Janson, C. E. (2008). 'Grid Influence on the Propeller Open-Water Performance and Flow Field'. Schiffstechnik/Ship Technology Research **55**, pp. 87-96.

Bouziad, Y. A. (2006). Physical Modelling of Leading Edge Cavitation: Computational Methodologies and Application to Hydraulic Machinery. PhD Thesis, Ecole Polytechnique Federale de Lausanne, Lausanne, Switzerland.

Brennen, C. E. (1995). Cavitation and Bubble Dynamics. Oxford University Press.

ESTECO (2009). modeFRONTIER 4.2 Users Manual.

Gaggero, S. (2010). Sviluppo di un Metodo a Potenziale per l'Analisi delle Caratteristiche Idrodinamiche di Eliche Marine Cavitanti e Supercavitanti. PhD Thesis, Università degli Studi di Genova, Genova, Italy.

Huuva, T. (2008). Large eddy simulation of cavitating and non-cavitating flow. PhD Thesis, Chalmers University of Gothenburg, Gothenburg, Sweden.

Koop, A. H. (2008). Numerical Simulation of Unsteady Three-Dimensional Sheet Cavitation. PhD Thesis, University of Twente, Twente, The Netherlands.

Kunz, R. F., Boger, D. A., Stinebring, D. R., Chyczewski, T. S., Lindau, J. W., Gibeling, H. J., Venkateswaran, S., & Govindan, T. R. (2000). 'A preconditioned Navier-Stokes method for two-phase flows with application to cavitation prediction'. Computers and Fluids **29**(8), pp. 849 – 875.

Menter, F. R. (1998). 'Two-Equation Eddy-Viscosity Turbulence Models for Engineering Applications'. AIAA Journal **32**(8), pp. 1598-1605.

Merkle, C. L., Feng, J. & Buelow, P. E. O. (1998). 'Computational Modeling of the Dynamics of Sheet Cavitation'. Third International Symposium on Cavitation, Grenoble, France.

Morgut, M. & Nobile, E. (2009). 'Comparison of Hexa-Structured and Hybrid-Unstructured Meshing Approaches for Numerical Prediction of the Flow Around Marine Propellers'. The First International Symposium on Marine Propulsors smp'09, Trondheim, Norway.

Morgut, M., Nobile, E. & Biluš, I. (2010). 'Comparison of mass transfer models for the numerical prediction of sheet cavitation around a hydrofoil'. In Press: Int. Journal of Multiphase Flow.

Pereira, F., Salvatore, F. & Di Felice, F. (2004). 'Measurement and Modeling of Propeller Cavitation in Uniform Inflow'. Journal of Fluids Engineering **126**, pp. 671 – 679.

Rao, S. S. (1996). Engineering Optimization - Theory and Practice. John Wiley & Sons, Inc.,

Salvatore, F., Streckwall, H., & van Terwisga, T. (2009). 'Propeller Cavitation Modelling by CFD-Results from the VIRTUE 2008 Rome Workshop'. The First International Symposium on Marine Propulsors smp'09, Trondheim, Norway.

Schneider, G. E. & Raw, M. J. (1997). 'Control Volume Finite-Element Method for Heat Transfer and Fluid Flow Using Colocated Variables - 1. Computational Procedure'. Numerical Heat Transfer **11**, pp. 363-390.

Shen, Y. T. & Dimotakis, P. E. (1989). 'The influence of surface cavitation on hydrodynamic forces'. 22nd ATTC, St. Johns, Canada.

Singhal, A. K., Athavale, M. M., Li, H. & Jiang, Y. (2002). 'Mathematical Basis and Validation of the Full Cavitation Model'. Journal of Fluids Engineering **124**, pp. 617 – 624.

Vaz, G. N. V. B. (2005). Modelling of Sheet Cavitation on Hydrofoils and Marine Propellers using Boundary Element Methods. PhD Thesis, Universidade Técnica de Lisboa, Lisbon, Portugal.

Versteeg, H. K. & Malalasekera W. (2007). An Introduction to Computational Fluid Dynamics, The Finite Volume Method. Pearson Education Limited.

Zwart, P., Gerber, A. G. & Belamri, T. (2004).'A Two-Phase Model for Predicting Cavitation Dynamics'. ICMF 2004 International Conference on Multiphase Flow, Yokohama, Japan.